ELECTRONIC SUPPLEMENTARY INFORMATION

Modulating electrical conductivity of metal–organic framework films with intercalated guest π-systems

Zhiyong Guo,[†a] Dillip K. Panda,[†a] Krishnendu Maity,[a] David Lindsey,[a] T. Gannon Parker,[a] Thomas E. Albrecht-Schmitt,[a] Jorge L. Barreda-Esparza,[b] Peng Xiong,[b] Wei Zhou[c] and Sourav Saha*[,a]

[a]Department of Chemistry and Biochemistry, Florida State University, Tallahassee, FL 32306, USA

[b]Department of Physics, Florida State University, Tallahassee, FL 32306, USA

[c]NIST Center for Neutron Research, National Institute of Standards & Technology, Gaithersburg, MD 20899, USA

[†]Equal Contribution Authors

Corresponding Author Email: saha@chem.fsu.edu

Experimental Section

I. Materials

Starting materials, such as $Zn(NO_3)_2.6H_2O$, 1,2,4,5-tetrakis-(4-carboxyphenyl)benzene (TCPB) strut, precursors of *N,N′*-bis(4-pyridyl)-2,6-dipyrrolidinylnaphthalenediimide (BPDPNDI) pillar, ZnO/EtOH suspension (40 wt%), solvents, and electrolytes were purchased from Sigma-Aldrich, Acros Organic, EMD Chemicals, and Cambridge Isotope Laboratory, and used as obtained. FTO-glass slides were purchased from Hartford Glass Co. The electrodes (Ag/AgCl, Pt-mesh, Pt-disk, and glassy-carbon disc) and electrochemical cells were procured from BASi.

[Disclaimer: Certain commercial equipment, instruments, or materials are identified in this paper to foster understanding. Such identification does not imply recommendation or endorsement by the National Institute of Standards and Technology, nor does it imply that the materials or equipment identified are necessarily the best available for the purpose.]

II. Synthesis of and Characterization of BPDPNDI Pillar

BPDPNDI was synthesized from 1,4,5,8-tetracarboxylic dianhydride (NDA) in four-steps via modified literature protocols (Scheme S1). The ^1H and ^{13}C NMR spectra were recorded at 298 K in appropriate deuterated solvents using Bruker Avance 400 MHz and 700 MHz spectrometers. MALDI-TOF data were recorded on a Bruker Autoflex-II instrument. FT-IR spectra were collected on a Perkin Elmer Spectrum 100 FT-IR spectrometer. Elemental analysis was conducted on a PerkinElmer 240 CHN analyzer.

2,6-Dibromo-NDA (DBrNDA). NDA was first converted to DBrNDA via controlled bromination following a literature protocol.[1] Briefly, to a solution of NDA (2.68 g, 10 mmol) in concentrated H_2SO_4 (10 mL), a solution of dibromoisocyanuric acid (11.48 g, 20 mmol) in concentrated H_2SO_4 (10 mL) was added slowly and the resulting mixture was stirred at 100 °C for 15 h. After cooling the reaction mixture to room temperature, it was poured on ice and the resulting yellow precipitate was filtered and washed thoroughly with H_2O and hot MeOH to obtain DBrNDA as the major product (4.0 g, yield ≈ 95%). MS (MALDI, –ve mode), *m*/*z*: observed: 423.20 $[M]^-$, calculated: 423.82 $[M]^-$. This sparingly soluble intermediate was used in the next step without further purification.

2,6-Dibromo-NDI (DBrNDI). DBrNDA dianhydride was converted to corresponding diimide DBrNDI following a literature protocol.[2] A suspension of DBrNDA (4.0 g, 9.4 mmol) and NH_4OAc (15.5 g, 188 mmol) in AcOH (40 mL) was stirred under reflux for 3 h. After cooling the reaction mixture to room

temperature, the resulting yellow precipitate was filtered and washed thoroughly with AcOH (80 mL) and then diethyl ether (120 ml) to obtain DBrNDI (3.2 g, yield ≈ 80 %) as a yellow powder. MS (MALDI, –ve mode) *m*/*z*: observed: 421.24 $[M]^-$, calculated: 421.85 $[M]^-$. This sparingly soluble intermediate was carried over to the next step without further purification.

2,6-Dipyrrlo-NDI. A S_NAr reaction of DBrNDI with pyrrolidine following a literature protocol[1] afforded 2,6-bispyrrolo-NDI. Upon addition of pyrrolidine (20 mL) to yellow DBrNDI (2.0 g, 4.7 mmol) it immediately turned dark red and then purple. The mixture was then stirred under reflux for 16 h to drive the reaction to completion. After evaporating excess pyrrolidine with a rotary evaporator, the resulting purple solid was washed successively with copious amounts of hexanes and MeOH to remove the red impurity and obtain a reasonably pure, albeit sparingly soluble 2,6-dipyrrolo-NDI as a navy blue solid (1.5 g, yield ≈ 73 %). MS (MALDI, +ve) *m*/*z*: observed: 404.48 $[M]^+$, calculated: 404.15 $[M]^+$. This sparingly soluble intermediate was carried over to the next step without further purification.

BPDPNDI Ligand. The BPDPNDI pillar ligand was prepared by a slightly modified Cu(II)-mediated coupling reaction[3] between 2,6-dipyrrolodinyl-NDI and 4-pyridineboronic acid, which installed the pyridine groups on imide rings. To a suspension of 2,6-dipyrrlodinyl-NDI (1.3 g, 3.2 mmol), 4-pyridinylboronic acid (3.96 g, 32.3 mmol), $Cu(OAc)_2$ (5.83 g, 32.3 mmol), and molecular sieves (4 Å) in anhydrous DMAc (100 mL) purged with O_2 for 30 min, Et_3N (4.5 ml, 32.3 mmol) was added, and the resulting reaction mixture was stirred at 55 °C under an O_2 environment for 2 d. Additional amounts of 4-pyridinylboronic acid (1.98 g, 16.2 mmol), $Cu(OAc)_2$ (2.92 g, 16.2 mmol), and Et_3N (2.3 ml, 16.2 mmol) in DMAc (25 ml) were then added to the reaction mixture, which was stirred at 55 °C under O_2 environment for another 3 d. After 5 d, the reaction mixture was cooled to room temperature, filtered, and washed with DMF (100 mL) to obtain a blue solid residue, in which the desired product was trapped. This residue was boiled in $CHCl_3$ (250 mL × 3) and filtered hot to extract the crude product in the filtrate. After concentrating the crude product from the combined blue filtrates, it was purified by SiO_2 column chromatography ($CHCl_3$/MeOH 100:1 to $CHCl_3$/MeOH 100:1.5) to obtain pure BPDPNDI (0.72 g, yield ≈ 40 %) as a vibrant navy blue-colored solid. ^{1}H NMR (400 MHz, CD_3Cl, 25 °C): δ = 8.84 (dd, $4H_{pyridine}$), δ = 8.42 (s, $2H_{NDI\text{-}core}$), δ = 7.33–7.29 (m, $4H_{pyridine}$), δ = 3.49 (dd, $8H_{pyrrolidine}$), δ = 2.06 (m, $8H_{pyrrolidine}$) ppm. ^{13}C NMR (175 MHz, DMSO-d_6, 25 °C): δ = 162.81, 161.81, 160.90, 152.45, 151.02, 144.78, 125.17, 121.74, 114.64, 40.51, 31.05 ppm. MS (MALDI-TOF, +ve) *m*/*z*: Observed 558.95 $[M]^+$, $[M]^+_{calcd}$ = 558.60. Elemental analysis: Calculated for $(C_{32}H2_{26}N_6O_4)\cdot(CH_3OH)_{0.75}\cdot(H_2O)_{0.5}$: C 66.47, H 5.11, N 14.21; Found: C 66.90, H 4.98, N 14.14. IR (cm^{-1}): 2921 (m), 2876 (m), 2835 (m), 1692 (m), 1653 (s), 1564 (s), 1448 (s), 1415 (m), 1329 (m), 1313 (m), 1208 (s), 1137 (m), 901 (m), 776 (s).

III. Solvothermal Synthesis and Characterization of BMOF [Zn_2(TCPB)(BPDPNDI)]

BMOF Synthesis. A DMF (10 mL) solution of $Zn(NO_3)_2\cdot6H_2O$ (60 mg, 0.2 mmol), TCPB strut (56 mg, 0.1 mmol), and BPDPNDI pillar (56 mg, 0.1 mmol) placed in a 20 mL screw-capped vial was kept inside an 80 °C oven for 24 h.[4] After cooling down the reaction mixture to room temperature slowly over 6 h, rod-shaped, navy blue colored crystals suitable for SXRD analysis were obtained (60 mg, yield ≈ 35 %). On the basis of the crystal data and CHN elemental analysis (calculated for $C_{147}H_{305}O_{75}N_{33}Zn_2$: C: 45.67, H: 7.95, N: 11.95; observed: C: 45.71, H: 7.92, N: 11.90) the molecular formula of BMOF was calculated to be $[Zn_2(TCPB)\ (BPDPNDI)]\cdot(DMF)_{27}\cdot(H_2O)_{36}$. IR ($cm^{-1}$): 2929 (m), 2863 (m), 1654 (s), 1384 (s), 1253 (m), 1092 (s), 862 (m), 783 (s).

Crystal Structure Analysis of BMOF. Single-crystal X-ray diffraction (SXRD) data of rod-shaped BMOF crystals were collected on a Bruker D8 Quest X-ray diffractometer (MoKα, λ = 0.71073 Å). Indexing was performed using APEX2 (Difference Vectors method). Data integration and reduction were conducted with SaintPlus 6.01. Absorption correction was done by multiscan method implemented in SADABS. The structure was solved using SHELXL-2013 (direct methods) and refined using SHELXL-2013 (full-matrix least-squares on F^2) contained packages. The powder X-ray diffraction (PXRD) data

were recorded on a Panalytical X'Pert Pro diffractometer with CuKα radiation (λ = 1.5418 Å) operated at 45 kV and 40 mA with a scan rate of 1 °/min at room temperature.

To optimize BMOF structure, density functional theory (DFT) calculation was performed with a Quantum-Espresso package using Vanderbilt-type ultrasoft potential with Perdew-Burke-Ernzerhof (PBE) exchange correlation.[5] A cutoff energy of 544 eV and a 2×2×2 k-point mesh (generated by Monkhosrt-Pack scheme) were enough for the total energy to converge within 0.01 meV/atom.

The structure of BMOF was first solved partially based on the SXRD data, which revealed a noncatenated pillared paddlewheel (PPW) architecture consisting of layers of TCPB-linked Zn_2 paddlewheel nodes (in crystallographic *ab*-planes), coordinated axially by the pyridyl rings of linear BPDPNDI pillars along the *c*-axis. However, the atomic coordinates of fluxional pyrrolidine rings and naphthalenediimide core of BPDPNDI were not fully resolved from the experimental SXRD data largely due the presence of disordered solvent molecules in as-synthesized crystals. Nevertheless, the distances between the Zn-nodes in BMOF (16, 11, and 19 Å along the *a*-, *b*-, and *c*-axes, respectively) are fully consistent with the lengths and geometry of TCPB and BPDPNDI ligands, and its overall network connectivity and dimensions are identical to that of a known isostructural noncatenated PPW-MOF composed of dibromo-TCPB (DBTCPB) struts and DPNDI pillars that have the same lengths and geometry as the TCPB and BPDPNDI ligands present in BMOF. On the basis of this insight, we optimized the atomic positions of pyrrolidine rings and naphthalenediimide core of BPDPNDI ligand in BMOF, using first-principle DFT calculations[5] to depict a complete picture of the noncatenated BMOF structure. The simulated PXRD pattern of this optimized BMOF crystal structure compares well with the experimental PXRD pattern of as-synthesized bulk material, validating the structural model. Cambridge Crystallographic Data Centre (CCDC) contains the supplementary crystallographic data of BMOF presented in this paper, which can be obtained free of charge via www.ccdc.cam.ac.uk/data_request/cif.

The PXRD profile of BMOF shows [001] refection at $2\theta \approx 4°$, which corresponds to the distance between the layers of the TCPB-linked Zn_2 paddlewheel nodes and is correlated to the lengths of the axially coordinated pillar ligands that connect these layers. This signal matches perfectly with that of a known isostructural noncatenated [Zn_2(DBTCPB)(DPNDI)] MOF[4] that has the same dimensions as BMOF, but a doubly interpenetrated [Zn_2(TCPB)(DPNDI)] MOF does not display this signal.[4] Like other bulky pillars,[6] bulky BPDPNDI was able to prevent catenation in a BMOF when used in conjunction with TCPB strut. The PXRD analyses further showed that while as-synthesized and $MeNO_2$-exchanged BMOFs are highly crystalline materials, they lose crystallinity upon evacuation of solvents, but regains this feature after being re-soaked in DMF, indicating that structural integrity of BMOF remains intact under ambient conditions and upon solvent loss (Fig. S1). The PXRD profile of BMOF microcrystals soaked in a methyl viologen solution ($MV^{2+}\cdot 2PF_6^-$, 30 mM/$MeNO_2$) for several days remained practically unchanged (Fig. S1), indicating that the structure of BMOF remained intact after MV^{2+} doping.

Thermogravimetric analysis (TGA). The TGA profile of BMOF was recorded under a N_2 atmosphere with a heating rate of 5 °C/min using a TA Instrument Q50 thermogravimetric analyzer.

Gas Adsorption Analysis. A Micromeritics ASAP 2020 surface area analyzer was used to measure CO_2 (Airgas, ultra-high purity grade) adsorption isotherms of BMOF. As-synthesized BMOF crystals were first washed with fresh DMF six times over 3 days. To replace DMF, BMOF crystals were then soaked in more volatile THF and the solvent was refreshed several times over 3 days. The THF-soaked BMOF powder was activated under high vacuum at room temperature for 24 h until the outgas rate was <5 μmHg/min prior to measurements. The activated BMOF sample was used for the CO_2 sorption measurement. The sorption measurement was conducted at constant 273 K maintained with an ice-water bath. The CO_2 uptake capacity of BMOF is 65 cm^2/g at 273 K, 1 bar (Fig. S3), which is comparable to that of isostructural [Zn_2(DBTCPB) (DPNDI)],[4] indicating its permanent porosity.

IV. Preparation and Characterization of BMOF Films and Devices

Preparation of ZnO Films. Annealed ZnO-coated conducting (FTO) or nonconducting glass slides were used to grow uniform BMOF films. The FTO-coated and nonconducting glass slides (ca. 6 cm × 4 cm) were first covered along the two opposite lengths with four layers of scotch tapes creating a 1 cm wide margin on each side and an exposed rectangular area (ca. 6 cm × 2 cm) in the middle. A ZnO/EtOH suspension (40 wt%, ZnO particle size ~130 nm, Sigma Aldrich) was then spin-coated (1000 rpm, 50 s) on the exposed midsections of these slides using a Laurell Technologies spin-coater, the scotch tape-covered margins remained ZnO-free. After removing the tapes, the ZnO-coated slides were annealed at 350 °C for 30 min in a Vulcan 3-550 PD programmable oven and then cooled slowly to room temperature to obtain smooth, transparent, and uniform ZnO films covering the rectangular midsections (6 cm × 2 cm). These slides were then cut into smaller pieces (the final dimension of slides: ca. 4 cm × 1.1 cm; the ZnO-coated area: 2 cm × 1.1 cm in the middle) that were used for growing BMOF films or for depositing Au electrodes before growing BMOF films on the exposed ZnO-covered areas.

Depositing Au Electrodes on ZnO-Glass Films. In order to incorporate BMOF films into electrical devices and to measure their electrical conductivity by four-probe method,[7] four Au electrodes (~100 nm thick Au pads on top of ~10 nm thick Ti pads) were deposited 1 mm apart through thermal evaporation technique (Edward Auto 306 Vacuum Coater) on ZnO-coated nonconducting glass slides covered with patterned stainless steel shadow masks (1 cm × 1 cm). After depositing the Au-electrodes on annealed ZnO films, the exposed ZnO-covered areas were available for growing BMOF films.

Preparation of BMOF Films and Devices. In order to grow BMOF films, DMF (10 ml) solutions of $Zn(NO_3)_2.6H_2O$ (15 mg, 0.5 mmol), TCPB (14 mg, 0.25 mmol), and BPDPNDI (14 mg, 0.25 mmol) taken in 20 mL screw-capped vials were placed in an oven preset at 80 °C for 2 h to initiate the formation of BMOF. Once the BMOF microcrystals started to form in the precursor solutions, the ZnO films were immersed into them at upright position or in a slightly slanted fashion with the ZnO-coated side facing down to prevent precipitation of BMOF crystals on the active side. The entire setups were then kept in an 80 °C oven for different durations. The ZnO-coated areas became selectively covered with uniform BMOF films within 0.5–1 h of growth period and the thickness of BMOF films increased gradually with longer immersion time. The rest of the areas that did not have an exposed ZnO layer, i.e., the bare FTO and glass areas as well as the Au-electrodes deposited on the ZnO layer remained completely BMOF-free. The initial formation of BMOF in solution ensured a rapid growth of its films on ZnO surfaces. Typically, the slides were withdrawn from the reaction medium after allowing film growth for ca. 1 h to obtain uniform blue films of BMOF on the ZnO-coated areas. These BMOF films and devices were then soaked in fresh DMF to remove any unreacted precursors that may have been trapped, and then immersed in $MeNO_2$ to remove DMF before drying and/or immersing into guest solutions. The BMOF/ZnO films stored in DMF or $MeNO_2$ at room temperature remain intact for months. The PXRD profile of blue films grown on ZnO-coated slides matched with that of as-synthesized bulk BMOF microcrystals deposited in vials, confirming that the blue films are indeed made of the same material.

Doping BMOF Films with Guest π-Systems. The BMOF/ZnO films were immersed into MV^{2+}, 1,5-difluoro-2,4-dinitrobenzene (DFDNB), dinitrotoluene (DNT) (30 mM / $MeNO_2$), and C_{60} (saturated in toluene) solutions to allow the appropriate guest molecules to enter into BMOF. While MV^{2+}, DFDNB, and DNT were able to penetrate into BMOF, as reflected from the enhanced conductivity of BMOF films doped with these guests, large C_{60} was size-excluded and did not influence the BMOF's conductivity.

Field-Emission Scanning Electron Microscopy (FE-SEM). Morphologies and the thickness of ZnO, BMOF, and doped BMOF films were analyzed by JEOL SM 7401F high resolution FE-SEM. For cross-sectional SEM analysis, BMOF films were sputtered with a conducting Pt layer (~3 nm). SEM images (Fig. S4) also show that the crystalline morphology of BMOF films remained intact after being doped with guest π-systems.

V. Electrical and Optical Measurements of BMOF Films Before and After Doping with Guests

UV/Vis Spectroscopy. The UV/Vis spectra of BPDPNDI, BMOF films (undoped and doped) were recorded on a PerkinElmer Lambda-25 UV/Vis spectrophotometer. While the absorption spectra of BMOF/ZnO films are essentially identical to that of the BPDPNDI ligand, the MV^{2+}-doped BMOF films show prominent, albeit broad and weak as expected, charge-transfer (CT) bands in the NIR region, indicating CT interaction between electron rich BPDPNDI pillars and electron deficient MV^{2+} guests.

Electrochemical analysis. Cyclic voltammograms (CV) of BPDPNDI, MV^{2+}, DFDNB, and DNT (1 mM solutions in 0.1 M Bu_4NPF_6 / MeCN) were recorded (Fig. S5) at room temperature on a Princeton Applied Research VersaStat-3-200 potentiostat/galvanostat instrument using a standard electrochemical cell, consisting of a glassy carbon as working electrode, Pt-wire counter electrode, and Ag/AgCl reference electrode. CV of BMOF was recorded using a BMOF/ZnO-FTO film as working electrode, Pt-mesh as counter electrode, Ag/AgCl as reference electrode, and a 0.1 M Bu_4NPF_6 solution as a supporting electrolyte. The redox potentials of BMOF match closely with that of redox-active BPDPNDI ligand.

Conductivity Measurement. To determine electrical conductivity (σ) of BMOF films (before and after exposure to different guest π-systems) the current-voltage (*I*-*V*) relationships of ZnO-glass and BMOF/ZnO-glass devices equipped with four Au electrodes were measured at room temperature and under ambient conditions (Table S1) through standard four-probe technique[7] using Kiethley 2400 source meter and LabView program. Before measuring the *I*-*V* relationship of the devices, the Au-plated areas outside the active device areas (ZnO and BMOF/ZnO) were scraped off to eliminate the possibility of any current leakage. The total electrical resistance ($R = V/I$) of at least three devices of each type—(i) bare ZnO film, (ii) undoped BMOF/ZnO film, and BMOF/ZnO films soaked separately in (iii) MV^{2+}, (iv) DFDNB, (v) DNT, and (vi) C_{60} solutions—were measured from the output voltage (V) between two inner probes in response to current applied (I) at the two outer electrodes under the same conditions. Since the BMOF and ZnO layers in BMOF/ZnO devices constitute two parallel connections between the Au-electrodes and charges can move between the electrodes through both of these layers, the contribution of the ZnO layer (R_{ZnO}) measured from a bare ZnO device was mathematically eliminated from the total resistance of the BMOF-containing devices (R_{Device}) to extract the actual resistance of the BMOF films (before and after soaking in guest solutions), namely $R_{component}$, using equation 1: $R_{component} = R_{device} \cdot R_{ZnO} / (R_{ZnO} - R_{device})$. This treatment follows a standard protocol for determining an unknown resistance (R_1) in an electrical circuit consisting of two parallel resistances R_1 and R_2, when the net resistance (R) and R_2 are known [$R = R_1R_2 / (R_1 + R_2)$].

All devices of any given type displayed consistent values of resistance, and the average resistance of each component ($R_{component}$) derived from equation 1 was used to calculate its electrical conductivity ($\sigma_{component}$) using equation 2: $\sigma_{component} = d / R_{component} \cdot t_{film} \cdot l$, where d = probe-spacing, t_{film} = film thickness measured by CS-SEM, and l = the effective length of Au electrodes (Table S1). The conductivity of each undoped and doped BMOF films was also calculated from the resistance of individual devices after eliminating the contribution of the underlying ZnO layer. The conductivity values of any given component obtained from three identical devices (Table S2) are in excellent agreement with each other and with the average value calculated from the average resistance of the corresponding material (Table S1).

The electrical conductivity of the undoped BMOF films is 5.8×10^{-5} S/m. Upon soaking in MV^{2+} solutions (30 mM/$MeNO_2$) the conductivity of the MV^{2+}-doped BMOF films increased gradually with longer immersion time, displaying 17-fold (0.98×10^{-3} S/m) and 34-fold (1.95×10^{-3} S/m) improvements after 24 and 48 h, respectively, before reaching the saturation point at 2.3×10^{-3} S/m after 70 h soaking, which accounted for an impressive ~35-fold upsurge from undoped BMOF films (6.8×10^{-5} S/m). Similarly, the conductivity of BMOF films soaked in DFDNB and DNT solutions (30 mM/$MeNO_2$ for 24 h) reached 3.5×10^{-4} S/m (a 6-fold improvement from the undoped BMOF films) and 1.5×10^{-4} S/m (a

2.6-fold upsurge), respectively, and remained practically unchanged after a longer exposure to these dopants. These results suggested that the smaller guest molecules percolated into BMOF faster than larger MV^{2+}, as the conductivity of DFDNB and DNT-doped BMOF films reached the saturation point after a shorter immersion time than the MV^{2+}-doped BMOF films. In contrast, the conductivity of BMOF films soaked in a saturated C_{60}/toluene solution remained practically unchanged (4×10^{-5} S/m) even after a prolonged soaking (7 d), suggesting that the large C_{60} molecules were size-excluded by BMOF.

The conductivity of the MV^{2+}-, DFDNB-, and DNT-doped BMOF films after quick washing (by dipping the doped BMOF films into fresh solvents and withdrawing them immediately) remained practically unchanged from that of the corresponding unwashed films, suggesting that the intercalated guests molecules adhered to the BPDPNDI pillars did not leak out readily. However, after soaking the doped BMOF devices in fresh solvents for a prolonged time (72 h), their conductivity values dropped significantly, i.e., close to that of the undoped BMOF films, indicating a gradual loss of the guest molecules from its pores. For example, after soaking the MV^{2+}- and DNT-doped BMOF films in fresh solvents for several days, their conductivity went down to ca. 3.75×10^{-5} S/m, a value that is closer to that of undoped BMOF films than the fully doped ones. Upon soaking blank devices, i.e., those devoid of BMOF/ZnO films in these dopant solutions, their *I-V* relationships did not display any measurable changes, as they fell beyond the detection limit of the Keithley source meter. These results suggest that MV^{2+}, DFDNB, and DNT themselves have extremely low conductivity values that are practically impossible to measure, which is fully consistent with the highly insulating nature of the redox-active small organic molecules. These experiments served as nice controls showing that these guests were able to enhance the conductivity of the BMOF films only after being intercalated between the preorganized BPDPBDI pillars, which improved electron delocalization through the resulting π-stacks.

Energy Dispersive X-ray Spectroscopy (EDS). To verify the influx of $MV^{2+}\cdot 2PF_6^-$ into BMOF, EDS data (Fig. S7) were collected using a JEOL 5900 SEM instrument coupled with a PGT Prism SiLi EDS detector calibrated with AlKα and CuKα. The EDS spectrum of BMOF revealed all of its elements (Zn, C, O, and N), whereas the same doped with $MV^{2+}\cdot 2PF_6^-$ (after a quick wash with a fresh solvent to remove the extraneous guests) displayed additional diagnostic P and F signals confirming the presence of the dopant. It is worth noting that EDS is a semiquantitative method for heavy elements and does not reflect the actual amount of the lighter ones, but just their presence.

References:

[1] C. Thalacker, C. Röger and F. Würthner, *J. Org. Chem.* 2006, **71**, 8098.

[2] I. De Cat, C. Roger, C. C. Lee, F. J. M. Hoeben, M. J. Pouderoijen, A. P. H. J. Schenning, F. Wurthner and S. De Feyter, *Chem. Commun.* 2008, 5496.

[3] E. T. Chernick, M. J. Ahrens, K. A. Scheidt and M. R. Wasielewski, *J. Org. Chem.* 2005, **70**, 1486.

[4] O. K. Farha, C. D. Malliakas, M. G. Kanatzidis and J. T. Hupp, *J. Am. Chem. Soc.* 2010, **132**, 950.

[5] P. Giannozzi, S. Baroni, N. Bonini, M. Calandra, R. Car, C. Cavazzoni, D. Ceresoli, G. L. Chiarotti, M. Cococcioni, I. Dabo, A. D. Corso, S. D. Gironcoli, S. Fabris, G. Fratesi, R. Gebauer, U. Gerstmann, C. Gougoussis, A. Kokalj, M. Lazzeri, L. Martin-Samos, N. Marzari, F. Mauri, R. Mazzarello, S. Paolini, A. Pasquarello, L. Paulatto, C. Sbraccia, S. Scandolo, G. Sclauzero, A. P. Seitsonen, A. Smogunov, P. Umari and R. M. Wentzcovitch, *J. Phys.: Cond. Matter* 2009, **21**, 395502.

[6] (a) T. Gadzikwa, O. K. Farha, C. D. Malliakas, M. G. Kanatzidis, J. T. Hupp and S. T. Nguyen, *J. Am. Chem. Soc.* 2009, **131**, 13613; (b) W. Bury, D. Fairen-Jimenez, M. B. Lalonde, R. Q. Snurr, O. K. Farha, J. T. Hupp, *Chem. Mater.* 2013, **25***,* 739.

[7] (a) L. B. Valdes, *Proc. IRE* 1954, **42**, 420; (b) F. M. Smits, *Bell Syst. Tech. J.* 1958, **37**, 711; (c) F. Gándara, F. J. Uribe-Romo, D. K. Britt, H. Furukawa, L. Lei, R. Cheng, X. Duan, M. O'Keeffe and O. M. Yaghi, *Chem. Eur. J.* 2012, **18**, 10595.

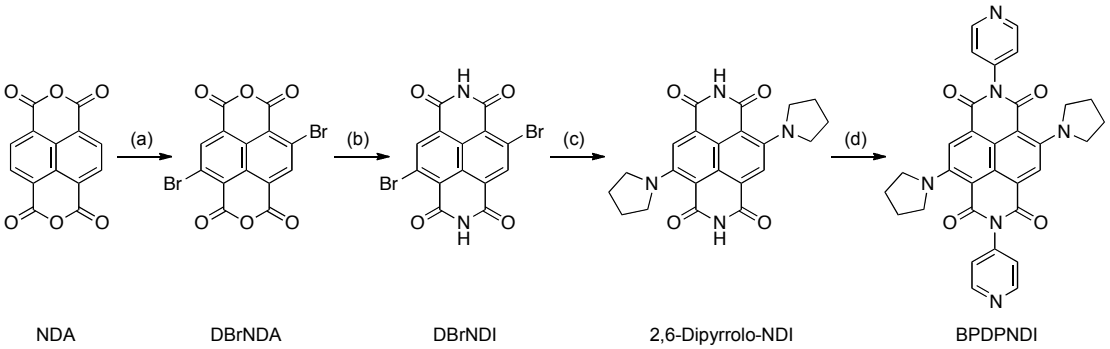

Scheme S1. Synthesis of BPDPNDI ligand: (a) dibromoisocyanuric acid, conc. H_2SO_4, 110 °C, 15 h (~95 %); (b) NH_4OAc, AcOH, reflux, 3 h (~80 %); (c) pyrrolidine, reflux, 16 h (~73 %); (d) 4-pyridinylboronic acid, $Cu(OAc)_2$, Et_3N, molecular sieves (4 Å), DMAc, 55 °C, 5 d. (40%).

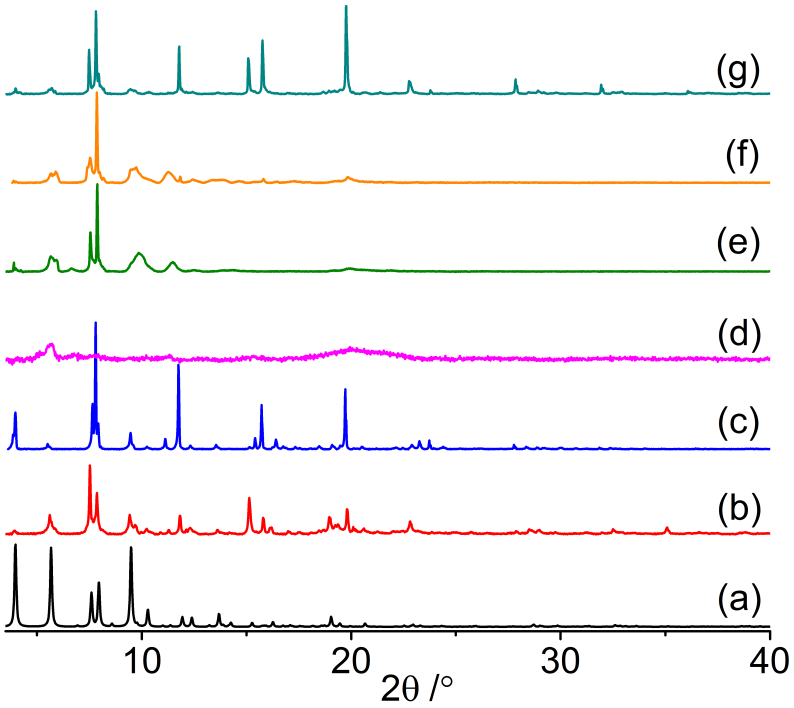

Fig. S1. PXRD profiles of (a) BMOF, simulated from SXRD data, (b) bulk as-synthesized BMOF powder (experimental), (c) known noncatenated isostructural [Zn_2(DBTCPB)(DPNDI)] PPW-MOF powder for a comparison, (d) fully evacuated BMOF, (e) BMOF powder exchanged with $MeNO_2$, (f) MV^{2+}-doped BMOF powder, (g) after re-soaking the evacuated BMOF powder in DMF.

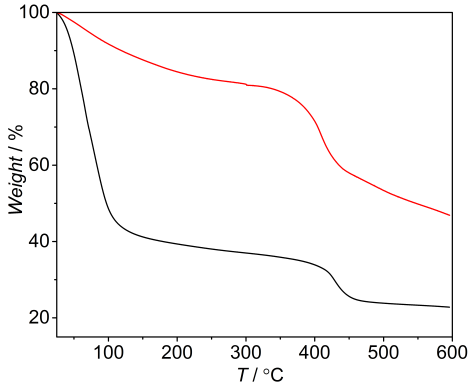

Fig. S2. The TGA profiles of BMOF (black: as synthesized, red: evacuated) show ~70% weight loss at 135 °C due to DMF loss.

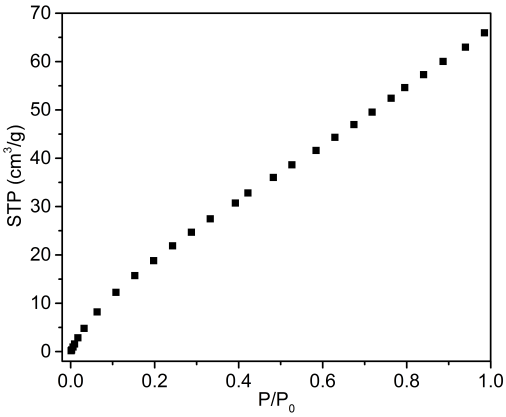

Fig. S3. The CO_2 adsorption capacity of BMOF at 273 K shows its permanent porosity.

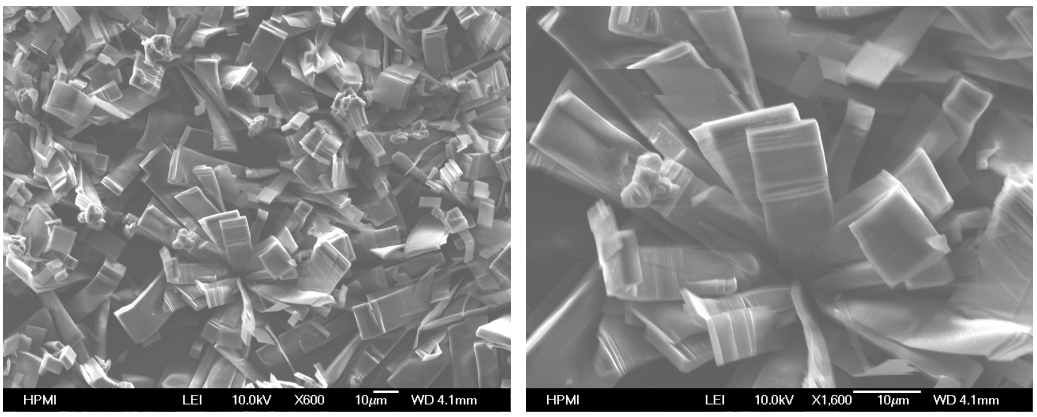

Fig. S4. SEM images of doped BMOF films show that their crystalline layered structures remain intact after being exposed to ambient conditions.

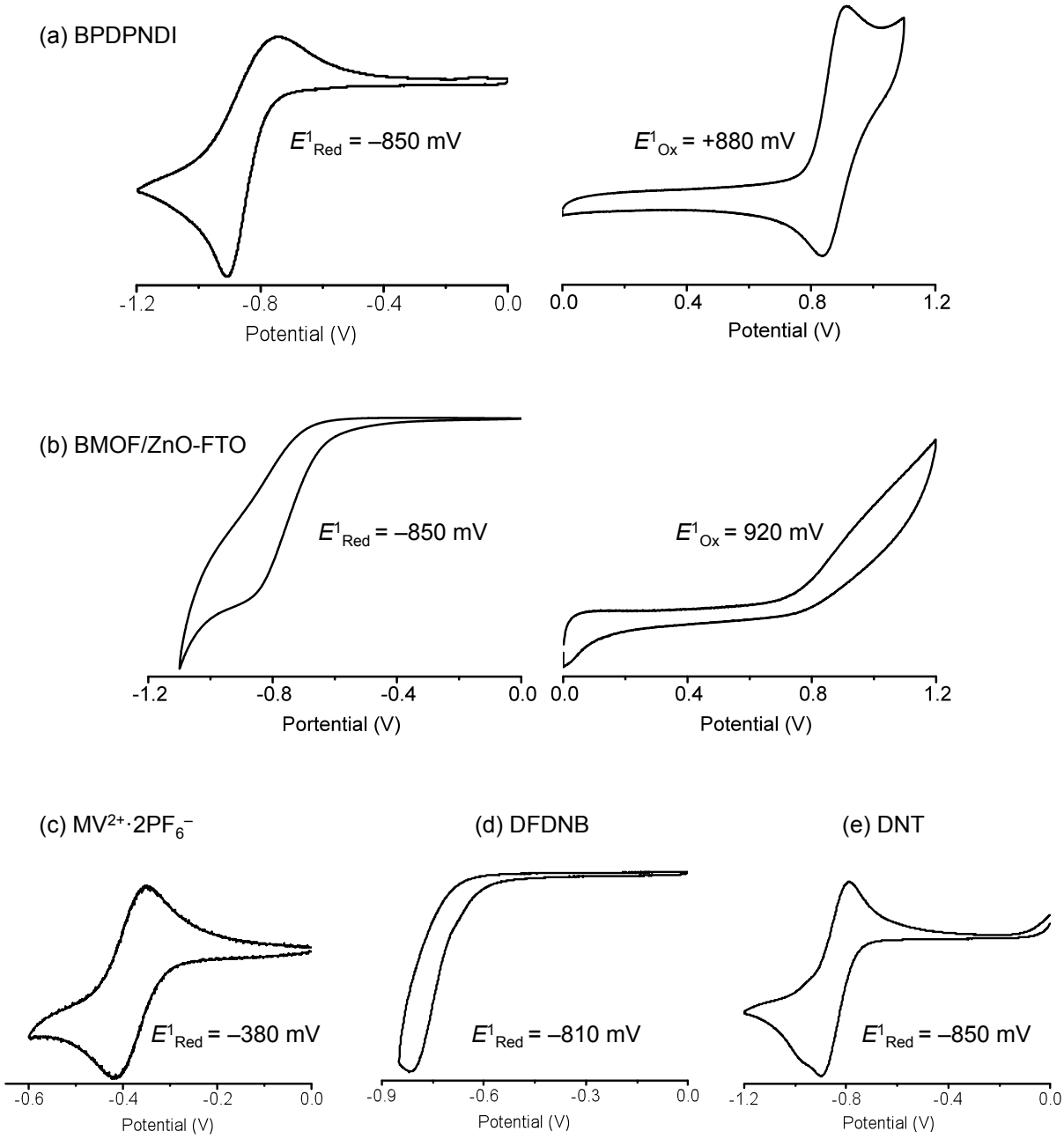

Fig. S5. Cyclic voltammograms (vs. Ag/AgCl) of (a) BPDPNDI ligand (1 mM in 0.1 M Bu_4NPF_6/ MeCN): left: reduction, right: oxidation, (b) BMOF/ZnO-FTO film: left: reduction, right: oxidation, (c) $MV^{2+}\cdot 2PF_6$ (0.5 mM in 0.1 M Bu_4NPF_6 / MeCN), (d) DFDNB(1 mM in 0.1 M Bu_4NPF_6 / MeCN), and (e) DNT (1 mM in 0.1 M Bu_4NPF_6 / MeCN).

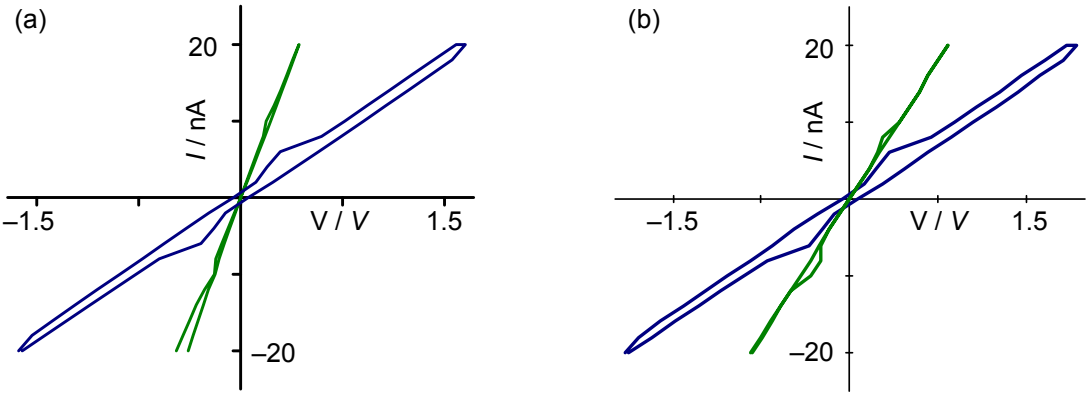

Fig. S6. Current-Voltage (*I*-*V*) relationship of BMOF-ZnO films: blue: undoped and green: doped with (a) DFDNB and (b) DNT guests.

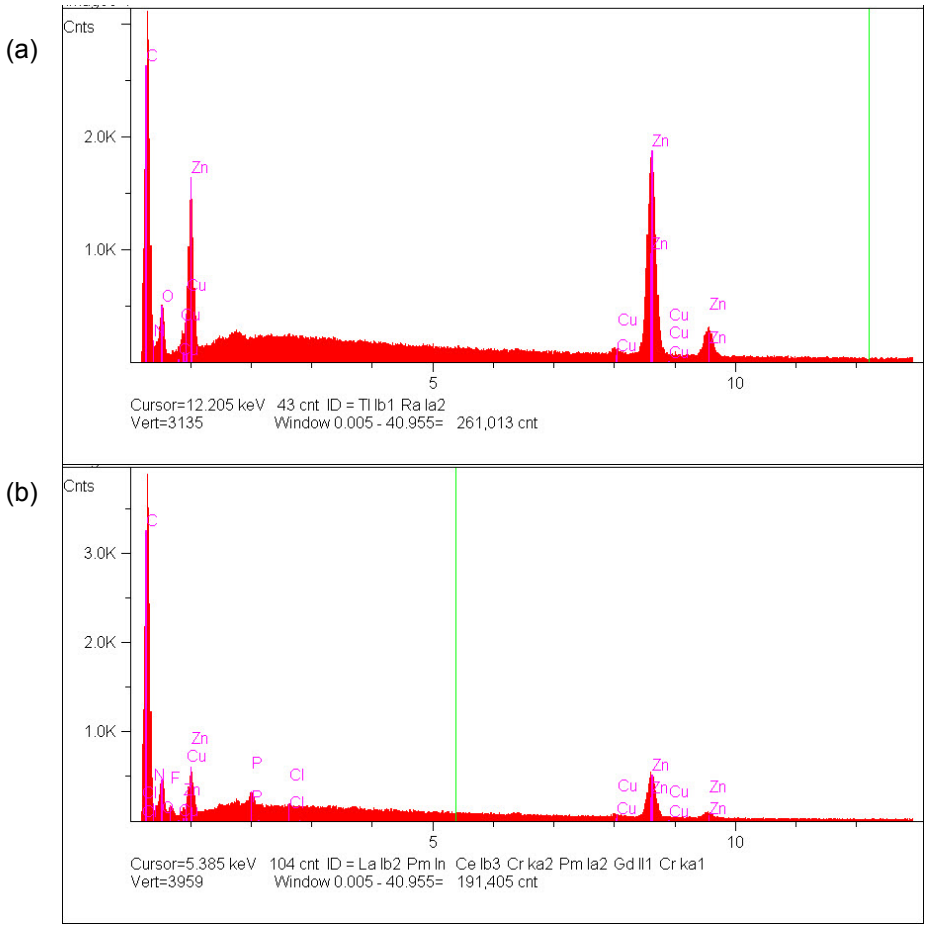

Fig. S7. The EDS spectra of BMOF (a) before and (b) after being doped with ($MV^{2+}\cdot 2PF_6^-$).

Table S1. Electrical measurements of ZnO and BMOF/ZnO devices before and after soaked in different guest solutions. The net electrical resistance (R_{Total} = V/I) of ZnO-glass and BMOF/ZnO-glass devices (before and after soaking in different guest solutions) were measured under ambient conditions (25 °C) through four-probe method: i.e., from output voltage (V) between two inner probes in response to applied current (I) between two outer electrodes. Since the BMOF and ZnO films in BMOF/ZnO devices constitute two parallel connections between the Au-electrodes, the contribution of BMOF films before and after soaking in guest solutions—i.e., $R_{component}$—was determined using the equation: $R_{component} = R_{Total} \cdot R_{ZnO} / (R_{ZnO} - R_{Total})$. Based on the resistance of individual components ($R_{component}$), and taking the thickness (t_{film}) of ZnO (~3 μm) and BMOF films (~20 μm), probe-spacing (d: 1.6 mm (center-to-center) for bare ZnO films, 1 mm (edge-to-edge) for BMOF films grown on ZnO films pre-patterned with Au electrodes), and the effective length of Au electrodes (l = 4 mm) into account, electrical conductivity ($\sigma_{component}$) of each component was derived from the equation: $\sigma_{component} = d / R_{component} \cdot t_{film} \cdot l$

Four-Terminal Electrical Devices	**R_{Device} (MΩ)**	**Device Components**	**$R_{Component}$ (MΩ)**	**$\sigma_{Component}$ (10^{-4} S/m)**
ZnO-glass	220 ± 9.6	ZnO	220	6.3
BMOF/ZnO-glass (Before soaking in any guests)	109 ± 1	BMOF Film (Undoped)	216	0.6
BMOF/ZnO-glass soaked in MV^{2+} (30 mM / $MeNO_2$) for 70 h	5.3 ± 0.8	MV^{2+}-Doped BMOF Film	5.4	23
BMOF/ZnO-glass soaked in DFDNB (30 mM / MeNO2) for 44	31 ± 4.3	DFDNB-Doped BMOF Film	36	3.5
BMOF/ZnO-glass soaked in DNT (30 mM / $MeNO_2$) for 48 h	60 ± 6.5	DNT-Doped BMOF Film	83	1.5
BMOF/ZnO-glass soaked in C_{60} (saturated/PhMe) for 7 d	132 ± 10.9	C_{60}-soaked BMOF Film	325	0.4

Table S2. Electrical conductivity (σ) of undoped and doped BMOF films from individual devices:

Films	**Sample 1 σ (S/m)**	**Sample 2 σ (S/m)**	**Sample 3 σ (S/m)**	**Average σ (S/m)**
ZnO	6.59×10^{-4}	6.07×10^{-4}	6.15×10^{-4}	$(6.3 \pm 0.3) \times 10^{-4}$
BMOF (Undoped)	5.60×10^{-5}	5.86×10^{-5}	5.89×10^{-5}	$(5.8 \pm 0.2) \times 10^{-5}$
MV^{2+}-Doped BMOF	1.96×10^{-3}	2.34×10^{-3}	2.65×10^{-3}	$(2.3 \pm 0.3) \times 10^{-3}$
DFDNB-Doped BMOF	4.21×10^{-4}	3.22×10^{-4}	3.12×10^{-4}	$(3.5 \pm 0.6) \times 10^{-4}$
DNT-Doped BMOF	1.33×10^{-4}	1.53×10^{-4}	1.71×10^{-4}	$(1.5 \pm 0.2) \times 10^{-4}$
C_{60}-soaked BMOF	4.80×10^{-5}	4.81×10^{-5}	3.48×10^{-5}	$(4.4 \pm 0.7) \times 10^{-5}$